

Modeling, Design, and Control of the Rehab-Exos, a Joint Torque Controlled Upper-Limb Exoskeleton

Domenico Chiaradia*, Massimiliano Solazzi*, Rocco Vertechy†, and Antonio Frisoli*

Abstract—In the last two decades, the research on exoskeletons has been increasing for several applications. The mechanical architecture of the exoskeleton directly influences its performances in term of torque and position control. An other aspect is the complexity of the joint design and the number of the required actuators and sensors per joint. In this work we present an This work presents a new upper-limb exoskeleton designed design endowed with compact elastic joints with torque sensors based on strain gauges. The torque sensor performance and the design aspects that affect the unwanted non-axial moment load crosstalk are addressed in this study. The joints have a high reduction ratio and they can display an output torque of 150 Nm, nevertheless, they are transparent by control and show exhibiting a low error in both haptic force rendering and position control. Good transparency and force rendering are obtained by model-based

To improve transparency a new state-feedback interaction torque control that takes into account the multi-dof non linear system dynamics and provides a compensation of non-linear effects such as friction and gravity components is proposed, in order to achieve an accurate estimation of human interaction force. To validate the proposed control as well as the chosen mechanical architecture, the full-state feedback control .The control schema takes into account part of the torque sensor non-linearities. Performances have been evaluated using different controls showing that this solution is a valid trade-off among exoskeleton complexity, maximum torque , was compared with two other benchmark state-feedback controllers, in two tasks of the zero desired force tracking (transparency) and contact with a virtual stiff wall (haptic rendering). The transparency benchmarking test was performed experimentally with 10 subjects at two different reference velocities. In both experimental conditions, the proposed joint torque control allows achieving higher performance both in term of transparency and haptic capabilities rendering, demonstrating how an active impedance by control can reach optimal performance if suitable state feedback is employed.

Index Terms—Joint torque sensor, elastic joint, upper limb exoskeleton, full-state feedback control, transparency, haptic rendering

I. INTRODUCTION

Exoskeletons are robotic interfaces for human-robot interaction where the highest physical symbiosis with the human operator is achieved . Unlike many industrial robots designed to exhibit a stiff structure and behavior, therefore to be used with a rigid position control, the exoskeletons are in direct contact with humans, so that they have to satisfy safety

*D. Chiaradia, M. Solazzi and A. Frisoli are with the PERCRO Laboratory, TeCIP Institute, Scuola Superiore Sant'Anna, Pisa, Italy. E-mail: d.chiaradia@santannapisa.it.

†R. Vertechy is with the DIN-Department of Industrial Engineering University of Bologna, Bologna, Italy. E-mail: rocco.vertechy@unibo.it.

Manuscript received xxx,yy,2018; revised xxx,yy,2018

and compliance requirements . In the common to physical Human-Robot Interaction (pHRI) devices [?].

In physical Human-Robot Interaction applications, moreover there are other performance measures inherently depending on the actuation and control that need to be considered, among which the two most relevant ones are transparency and haptic rendering:

Transparency relates to the ability of the robotic system interacting with a human who is moving voluntarily not to apply any assistance/ resistance to free motion [?], or equivalently means that the robot's reaction forces perceived by the user are minimal [?]. No standard procedures exist for the measurement of transparency in pHRI, but for exoskeletons there is a general consensus to refer not only to end-effector resistance forces, but also to single joints resistance torques or measurements at contact points [?].

Haptic rendering refers to the capability of the device to render a desired dynamic behavior, such as a virtual impedance or a virtual wall, i.e. a task featuring both very high impedance (when in contact with the wall) and very low impedance (when out of contact) [?]. Better mechanical structures, including appropriate dimensioning of the sensors and actuators, combined with more effective control strategies should predict the maximum stiffness that can be displayed by existing devices [?].

In the last two decades, several exoskeleton solutions have been proposed using different implementation principles accordingly according to the field of application. Some important applications of the exoskeletons are post-stroke neurorehabilitation [?], [?], assistance for limb movements, such as neurorehabilitation and assistance [?], [?], human power augmentation for lifting heavy loads [?] and teleoperation [?], [?] to enhance the master immersivity and dexterity. In human-robot interaction devices, telepresence [?], [?], [?], where different actuation systems and technologies have been exploited. Technologies based on geared solutions [?], [?], [?], tendon drives [?], [?], hybrid solutions (screw and cable actuators) [?] and on pneumatic or hydraulic actuation [?], [?] can be found in literature. However in human-robot interaction applications, a fundamental characteristic of the actuation systems is its compliance. The

As shown in Figure 1, the actuators found in recent exoskeletons and humanoids can be classified accordingly to [?] for pHRI can be mainly classified in two main categories, variable impedance actuators (VIA) and stiff actuators suitable for position control strategies. For HRI the use of purely

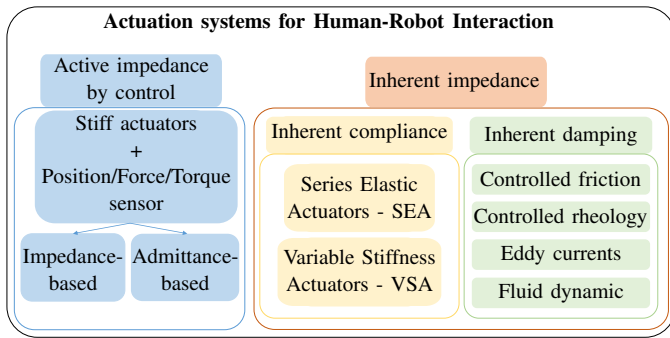


Fig. 1. Schema of variable impedance actuation systems for human-robot interaction. The impedance can be simulated and actively changed by control (this relies on position and torque sensors) or can be an inherent mechanical property of the actuator. In the latter case the mechanical stiffness can be a fixed value (SEA) or can be adjusted (VSA), and the damping can be controlled.

position controlled solution is of limited interest. On the other hand, a variable impedance can be obtained by control (called active impedance by control) or can be the active impedance by control and inherent impedance (compliance, damping) according to how they adjust the impedance displayed to the user, obtained either by control in the first case or as a mechanical property, also defined passive impedance (inherent compliance or inherent damping). shows a scheme of the two variable impedance typologies in the second case [?].

In inherent compliance systems inherent compliance actuators an electric motor is coupled with a spring with fixed (Series Elastic Actuator - SEA) or variable stiffness (Variable Stiffness Actuators – VSA). Inherent damping systems, based on the principle that adding a series elastic element reduces the peak power demand to the motor. Inherent damping actuators are based on the control of the friction by means of eddy currents, controlled rheology or fluid dynamic. Recently double actuation architectures have been developed for variable impedance actuators [?], coupling the stiff motor in parallel with the elastic element (Parallel Elastic Actuators - PEA) dynamics.

Both SEA and VSA have been implemented in exoskeleton as for example in Lopes [?], an exoskeleton for the gait assistance that is based on SEA actuation, or in NEUROexos elbow exoskeleton [?] that is based on VSA and in and ALTACRO locomotion exoskeleton [?] that introduces a Mechanically Adjustable Compliance and Controllable Equilibrium Position Actuator (MACCEPA).

All the variable impedance actuators have the advantage of absorbing impacts and SEA, PEA and VSA (inherent compliance) and VSA can eventually mechanically store energy during passive phases and release it in active phases of the movement cycle. In general, adding a series elastic element reduces the peak power demand on the motor. VSAs generally use two motors which increases the size, weight and complexity of the actuator in comparison with an SEA [?].

On the other side, active impedance systems are active impedance by control actuators are composed of electric mo-

tors coupled with a transmission/reduction system; they can be classified according to the backdrivability and sensing system. Force controlled actuators implement a force/torque sensor in the joint at the joint level and can achieve impedance behavior by closed-loop control. In general traditional actuators, due to the absence of with no elastic or damping elements, can be lighter and more compact than passive variable impedance actuators, but their time response and dynamic bandwidth is limited by control and electrical properties of actuators, such as maximum velocity of electrical motor. Schema of variable impedance actuation systems for human-robot interaction. The impedance can be simulated and actively changed by control (this relies on position and torque sensors) or can be an inherent mechanical property of the actuator. In the latter case the mechanical stiffness can be a fixed value (SEA) or can be adjusted (VSA), and the damping can be controlled.

The Rehab-Exos. It is a 5 DOF upper-limb exoskeleton with 4 actuated joints. The joints J_1 , J_2 and J_4 share the same characteristics: high reduction ratio (100:1) by means of harmonic drive, embedded torque sensor and maximum actuation torque of 150 Nm. The joint J_3 is composed by a semi-circular guide actuated by a DC motor through tendon transmission. Joint J_5 is passive and the exoskeleton is equipped of a force/torque sensor at the end effector that is used for evaluation purposes.

Solutions based on joint torque sensor have been proposed in the last years mostly for example in lower limb exoskeletons. In [?] and in [?] two knee exoskeletons based on joint torque sensor were presented; the latter exoskeleton implements an admittance control based on the torque sensor reads. In [?] the torque sensor for a lower limb exoskeleton allows to accurately estimate the human muscular torque that were exerted during the human-robot interaction [?], [?], [?]. The advantage of joint torque sensor based solutions is their compactness and robustness, but when the torque sensor is embedded in the joint it is sensitive to the link inertia in addition to the human interaction torques, thus affecting the system transparency. A mechanical solution is presented in [?] where the transparency of a lower-limb exoskeleton has been improved by positioning the force/torque sensor on the supporting cuffs, that is at the interaction point between the human leg and the exoskeleton. Even if SEA and VSA are less compact than traditional actuators, for example [?] proposed a solution based on a VSA for an exoskeleton of the leg that reduced the lateral size and integrates a torque sensor based on spring's deflection reads. Sensors used to measure these deflections are generally encoders [?] and potentiometers [?]; the latter usually require custom mechanical supports to avoid errors related with its sensitivity to misalignments. While the deflection based force estimation becomes a most widely utilized method for the SEAs and VSAs and performs fidelity force control performance in various robotic applications, there are still difficulties because of the practical issues such as spring deflection measurement error or noise of the encoder signal [?]. These factors have much negative impact on SEA with high stiffness. In [?], for example, a polymer optical fiber has been mounted on the torsional spring of a SEA to read angles and torques in a more accurate way without

considerably enlarging the size of the actuator at the cost of a more specific system electronics.

Thus, the ~~use adoption~~ of inherent compliant actuation systems rather than achieving compliance by control ~~systems~~ is not a trivial choice and it depends on the desired mechanical features and is the result of a trade-off among compactness, weight, simplicity, costs, safety, efficiency ~~and compliance~~. A good trade-off that prefer compactness, simplicity and uses just one motor is an active impedance by ~~control actuation system that integrates closed-loop control system that~~ an elastic component to transmit and to measure axial torques at the same time.

~~In this paper we address the issue of a collaborative robot behavior, by designing Based on the above, in this paper we introduce the design and the experimental characterization of the Rehab-Exos, an upper limb exoskeleton based on endowed with joint torque actuatorsendowing, based on joint torque sensors and extend our previously work presented in [?]. The Rehab-Exos allows to obtain a physical interaction characterized by good transparency and force rendering accuracy, it is capable to exert a wide range of forces and at the same time it exhibits high position accuracy due to high gear reduction ratio, high reduction ratio, and the design of an interaction joint torque control that maximizes both transparency and quality of haptic rendering.~~

The first part of the paper widely treats the critical issue due to the use of a torque sensor embedded in the joint and in particular the sensitivity to non-axial load has been studied. Then, in the second part the joint model and the control technique are presented. In particular, for what concern to improve transparency we propose an interaction torque control that take a new interaction state-feedback torque control (JTFC1) that takes into account the multi-dof non linear system dynamics and provide provides a compensation of other non-linear effects such as inertial, such as friction and gravity components, to achieve an accurate estimation of human interaction force. This is accomplished by a single joint optimum observer that ensures joint torque tracking, while a centralized control estimates and compensates for the dynamics of the whole system. Moreover, we have evaluated the effect of dynamic compensation on system transparency highlighting good results.

To validate the proposed control as well as the chosen mechanical architecture, the full-state feedback control ~~has been compared with a basic feedback control was compared with two alternative controllers, a feedback control (JTFC2) and a passivity-based feedback control (JTFC3), in two tasks: the zero desired force tracking (transparency) and the contact with a virtual stiff flat surface. For what concern wall (haptic rendering). The transparency benchmarking test among the 3 controllers was performed experimentally with 10 subjects and two different reference velocities, according to the evaluation procedure already tested in [?], in order to achieve comparable benchmark results.~~

As far as haptic rendering, we evaluate at geometrical level the quantitative and qualitative behavior of the stability behavior and quality of force rendering of the proposed controller and we was assessed through a virtual wall simulation

implemented with increasing stiffness values and compared it with the other two implemented controllers. Results reward the chosen mechanical and control strategy as presented in the last part of this paper. benchmark controllers. In both experimental conditions, the proposed joint torque control allows it to achieve higher performance both in term of transparency and haptic rendering, demonstrating how an active impedance by control can reach optimal performance if suitable state feedback is employed.

This paper is structured as follows: Section II presents the design of the Rehab-Exos with a particular focus on the strain gauge-based torque sensor design and issues. Section III-A provides a mathematical model of the single joint whereas in the Section III-B the full dynamics model of the Rehab-Exos is described. Section ?? explains the proposed full state feedback controller and recalls two torque controls benchmark torque controllers already known in literature. Section ?? presents the experiments and the obtained results. Finally, discussions and conclusions are addressed in Sections III and IV respectively.

II. SYSTEM DESIGN

The Rehab-Exos is an active robotic exoskeleton (Fig. ?? which is 2) designed with the idea to be compact modular, easily reconfigurable and to have with a good trade-off between transparency and force replication payload. It was conceived for rehabilitation applications and it is designed in such a way to generate controlled contact forces/torques not only at its end-link end-effector handle, but also at intermediate links contact points with the user arm. When the user is wearing the device he can control the full force interaction with the exoskeleton and guide/be guided involving all shoulder and elbow articulations of the arm(wrist, shoulder, elbow). The physical interaction between user and exoskeleton is monitored by the joint torque sensors which performances depend on several design and implementation aspects that are addressed in subsection II-B.

A. Mechanical design of the Rehab-Exos

As depicted in Fig. ?? and in 2, the exoskeleton has a serial architecture isomorphic with the human kinematics that comprises: a shoulder joint fixed in space and composed by three active joints J_1 , J_2 and J_3 ; an active elbow joint J_4 ; and a passive revolute joint J_5 allowing for wrist prono/supination. For a more detailed description of both Rehab-Exos and actuation groups, the reader can refer to [?]. A schematic representation of the Rehab-Exos exoskeleton:

CAD section of the J_1 , J_2 and J_4 joint actuator of the Rehab-Exos.

The three joints J_1 , J_2 and J_4 of the exoskeleton are motorized through identical actuation groups. Each joint features a custom-made frame-less brush-less torque motor integrating a compact Harmonic Drive (HD) component set. The actuator provides a joint output torque equal to 150 Nm with an overall weight equal to 3.7 Kg and a motor shaft inertia reduced to the joint output shaft $J_m = 3.7 \text{ Kgm}^2$ $J_m = 2.5 \text{ Kgm}^2$. The Harmonic Drive performs a reduction equal to 100:1. Due to the adopted mechanical components, the joints feature limited

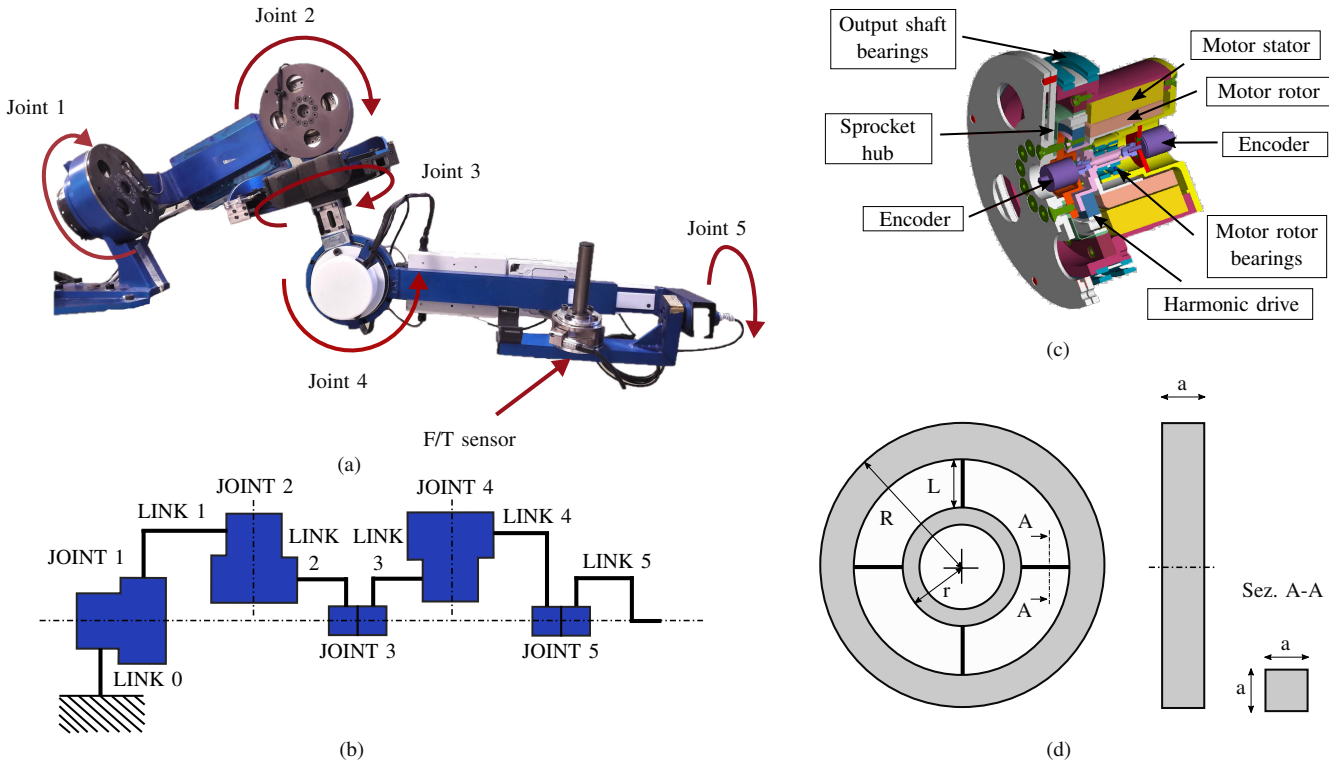


Fig. 2. (a) The Rehab-Exos. It is a 5 DOF upper-limb exoskeleton with 4 actuated joints. The joints J_1 , J_2 and J_4 share the same characteristics: high reduction ratio (100:1) by means of harmonic drive, embedded torque sensor and maximum actuation torque of 150 Nm. The joint J_3 is composed by a semi-circular guide actuated by a DC motor through tendon transmission. Joint J_5 is passive and the exoskeleton is equipped of a force/torque sensor at the end-effector that is used for evaluation purposes. (b) A schematic representation of the Rehab-Exos exoskeleton. (c) CAD section of the J_1 , J_2 and J_4 joint actuator of the Rehab-Exos. (d) Characteristic dimensions of the torque sensor.

back-drivability at motor power-off and limited mechanical complexity to ease maintenance as well as reduce costs. A CAD section of the J_1 , J_2 and J_4 joints is depicted in Fig. ??(c). Joint J_3 is characterized by a tendon transmission that is used to transmit the actuation torque through an open semi-circular guide. More detail on the joint J_3 can be found in [?].

B. Design aspects of the strain gauge based torque sensor

The three joints J_1 , J_2 and J_4 have a torque sensor featuring a four-spoke-shape geometry. Despite further augmenting the actuation group compliance, the availability of joint-torque sensors enables for multi-contact force control at multiple points distributed over the links and, additionally, makes it possible: 1) to close a stable high-bandwidth torque inner loop around each joint which is weakly affected by robot link variable inertia; 2) to suppress robot vibrations produced by the inherent transmission compliance (Harmonic Drive); 3) to reduce internal disturbance torques caused by actuator and reducer (for instance friction losses, actuator's torque ripples and gear teeth wedging actions); to measure externally applied forces/momenta and complex non-linear dynamic interactions between joints and links.

The sensor consists of two fully balanced strain gauge placed on different beams of the spoke, which is located at the joint output shaft. **Characteristic dimensions of the torque sensor:** The sensor is made by AISI 630 steel, an

TABLE I
CHARACTERISTIC DIMENSIONS OF THE TORQUE SENSOR

Dimension	Value [mm]
R	78
r	38
L	24
a	4
round radius	2

harmonic steel exhibiting yield strength of 1950 MPa, Young's modulus of 196 GPa and has been dimensioned to exhibit low weight and high sensitivity to axial moments. The axial torsional stiffness of the sensor is $k_s = 30 \text{ kNm/rad}$ and can be calculated as in (1).

$$k_s = \frac{\tau}{\theta} = \frac{Ea^4(r + L(1 - Q))}{3L^2(1/2 - Q)} \quad (1)$$

where the adimensional parameter Q is given by

$$Q = \frac{3r + L}{6r + 3L} \quad (2)$$

where, according to Fig. ??, **R** is the radius of the external sensor ring, **2 d**, **r** is the radius of the internal sensor ring, **L** is length of the beams and **a** is the side length of the beam section. The characteristic dimensions of the sensor are reported in TABLE I. Moreover, the overall

TABLE II
STRAIN OF THE 4 STRAIN GAUGES

Probe 1 [m]	Probe 2 [m]	Probe 3 [m]	Probe 4 [m]
1.65e-5	-1.33e-5	-1.91e-5	2.2546e-5

TABLE III
SENSOR READS TO NON-AXIAL MOMENTS

Applied Torque [Nm]	Sensor reads per angle [Nm]			
	0°	45°	90°	180°
32	1.6	2.4	2.2	2.3
64	2.9	4.8	4.4	4.4
96	4.5	7.5	6.9	6.9

joint torsional stiffness reduced to the joint output shaft is $k = 11.38 \text{ kNm/rad} = 11.38 \text{ kNm/rad}$.

The position of the strain gauges on the beam is a trade-off: if they were positioned in the middle of the beam the sensor sensitivity would be low, on the contrary, if they were positioned near the extremities the sensor reads would be affected by the non-linearities of the rounds of the beam. The selected distance from the extremities was $p = 1/8 L = 3 \text{ mm}$. To estimate the strain of the beam in a given point with distance p from the inner ring under a certain axial torque τ , the normal tension σ_p that acts on that point p needs to be computed as

$$\sigma_p = \frac{3\tau((1-Q)L-p)}{2a^3((1-Q)L+r)} \quad (3)$$

and then the strain follow as

$$\epsilon_A = \frac{\sigma}{E} \quad (4)$$

where E is the Young's modulus.

Theoretically, i.e. using (4), at 3 mm from the inner ring and under an axial torque of 120 Nm , a maximum strain of $2.7 \times 10^{-3} \text{ m}$ is obtained. The same test has been conducted using a FEM software tool (Ansys®) because the surface of the strain gauge is not negligible compared to the beam one (see Fig. 3) obtaining a maximum strain of $1.98 \times 10^{-3} \text{ m}$. The strain of each strain gauge when a 1 Nm load is applied can be shown in TABLE II.

An important characteristic of the torque sensor is the sensitivity to non-axial moments, thus an experimental test has been conducted to compute the sensitivity, i.e. a predetermined non-axial torque has been exerted on the sensor in 4 configurations (angle) of the sensor. Experimental results are reported in TABLE III and the sensitivity is equal to

$$S_S = \frac{C_{mis}}{C_S} = 0.067 \quad (5)$$

The sensitivity to non-axial moments is relatively high compared to one mentioned in [?].

The reason of these results has been investigated and two causes (or a combination of them) have been proposed. The first cause of error could be a strain gauges mounting misalignment. The second cause could be an excessive deformation

TABLE IV
STIFFNESS OF THE COMPONENTS

Component	Stiffness [kNm/rad]
K_{TS}	4.1
K_{HD}	0.4
K_B	23.6
K_{TOT}	24

of the sensor due to the non-axial moments. About the first hypothesis, the sensitivity of the strain gauges to non-axial load C_S (when a flexible model of the HD is considered) due to strain gauges misalignment can be modeled as

$$S_{misal} = k_s \cdot (k_{ex} \cdot e_x + k_{e\theta} \cdot e_\theta) \quad (6)$$

where k_s is a scaling factor equal to $7.87e^{-3}$, k_{ex} is the sensitivity to linear mounting misalignment equal to 3, $k_{e\theta}$ is the sensitivity to angular mounting misalignment equal to 2.3, whereas e_x and e_θ are the positional and angular misalignment errors respectively (see Fig. ??3 a)). Equation (6) and the measured sensitivity of 0.067 lead to a misalignment errors of millimeters and decades of degree, but these values are over the actual misalignment the installation operator may have introduced as it can be seen in Fig. ??3 b).

About the second hypothesis it is worth to notice that the sensor from a structural point of view is in series to the HD and this series is in parallel with a couple of bearings. This parallel chain composes a hyper-static system (see Fig. 4), therefore the excessive sensitivity may be due mounting misalignment of the mechanical parts of the chain.

For the study of the hyper-static system a linear elastic behavior of the system parts were supposed and the system response at non-axial moments was modeled as a mono-dimensional model as in ??.. The overall joint stiffness to non-axial moments K_{TOT} was experimentally evaluated, whereas the non-axial moment stiffness of the torque sensor K_{TS} and of the HD K_{HD} were computed via FEM analysis. The FEM results are depicted in Fig. 3 and the stiffness values are reported in table TABLE IV. For the FEM analysis a more dense grid mesh for the zone of interest has been used. For each area the average strain along the radial direction has been computed.

A possible mounting misalignment of the hyper-static chain may be a collinear and/or concentric mounting misalignment between the sensor axis and the bearing axis. In this case, the HD works as an universal joint that connect the sensor (that is connected to the $(n+1)$ th link) and the n -th link. The sensitivity to non-axial moments defined in equation (5) and the mechanical properties in TABLE IV lead to a theoretical mounting misalignment of about 0.5 mm , but this value is not in agreement with the design tolerances and components data-sheets from which a misalignment of about 0.05 mm results in the worst case.

To summarize, unwanted sensor reads to non-axial load may be due to the combination of effects from sensor mounting misalignments and HD excessive deformation.

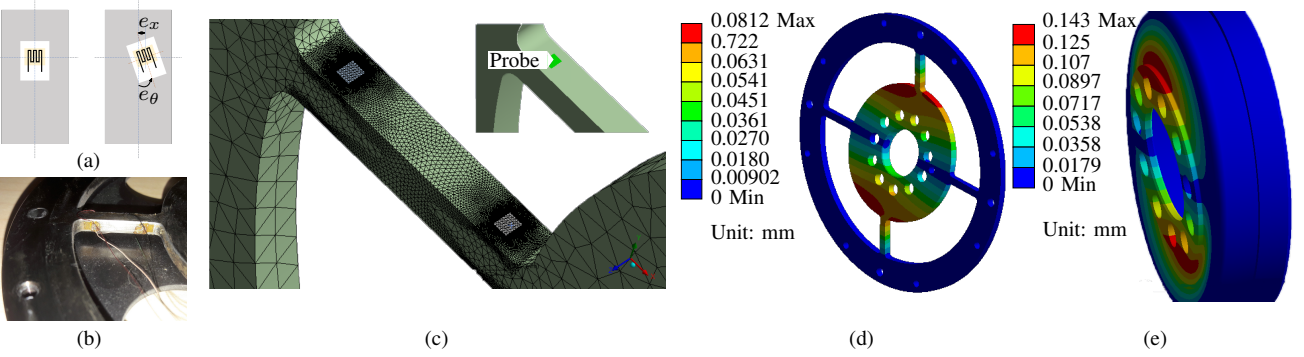


Fig. 3. A possible cause of high sensitivity to non-axial load is the strain gauges's mounting misalignment. The linear displacement e_x and the angular one e_θ are highlighted in (a). A detail of the mounted strain gauges on the torque sensor in (b). (c) For the FEM analysis a more dense grid mesh for the zone of interest has been used. For each area the average strain along the radial direction has been computed. (d) The FEM analysis results of the torque sensor, and of the flexible spline deformation under non-axial load (e).

In order to minimize this undesired effect ~~the authors propose a model-free adaptive~~ method based on artificial neural networks (ANN) to characterize and compensate this non-linear ~~behavior that results difficult to model, response of the sensors, in alternative to modeling approaches in reason of the complexity of the phenomenon.~~ Considering the ideal and linear ~~response of the~~ sensor, the torque readings can be expressed as $\tau_s = k_v * v$, where v is the measured voltage tension and k_v is the torque sensor's voltage constant. In the real case it be can written $\hat{\tau}_s = k_v * v + \delta\tau$, where $\delta\tau$ is the non-linear influence on the sensor readings due to the mounting and non-axial loads. By experimental evidence, it's possible to assert that the term $\delta\tau$ varies in a non-linear way with respect the exoskeleton pose (joint angles) and load.

The mounting errors influence the torque readings non-linearly with respect to the joint angle, while the non-axial torques depends in part on the interaction with human and in part on the dynamics and gravitational torques acting on the considered joint. ~~The FEM analysis results of the torque sensor (a) and of the flexible spline (b) deformation under non-axial load.~~ For all the three sensors the k_v constants have been experimentally evaluated. In order to minimize the effect of non-linear undesired term $\delta\tau$, an ANN has been used. ANN is a mathematical approximation approach that is capable ~~to infer of inferring~~ non-linear behavior from experimental acquisitions. The ANN with 7 neurons in the hidden layer and sigmoid activation function are ~~deputed~~ employed to estimate the error on the basis of the 4 angles and load on each axis. The angular information is useful to infer the assembly error component, whereas for the load influence the gravitational torque has been used.

To train the neural network the whole workspace has been partitioned in 414 target points. The torque sensor readings were acquired while the exoskeleton was holding the target position. For each joint, the training has been done using as input the 4 angles and the gravity torque that act on the joint (computed by model), and as output the residual value $\delta\tau = G_i(\theta_m) - k_v * v$, where G_i is the gravity load on the i -th joint when the pose is given by the angle vector θ_m . The set of target points was divided in 3 parts: 70% for the training

set, 20% for the validation set and 10% for the test set. The regression value between the ANN output and the target points is 0.99. The actual sensor torque estimation is given by $\bar{\tau}_s = k_v * v + \delta\tau(\theta_m, G_i)$, and a scheme of this estimation is shown in the ???. The estimated sensor torque is obtained as the sum of sensor's reading and the predicted undesired non-linear term. :

C. Control Hardware

The control architecture of the Rehab-Exos is decentralized and based on the EtherCAT communication bus in order to guarantee both optimal signal to noise ratio in the acquisition of analogical signals, i.e. force sensors, and higher standards of safety. The EtherCAT communication network consists of one master controller and four Ethercat Slave Controllers (ESC), one for each actuation joint. The master controller is handled by Simulink Real-TimeTM Operating System that executes the centralized control model at 2 kHz frequency.

Motors of the exoskeleton consist of three 170 VDC power supplied brush-less motors on the 1st, 2nd and 4th joint each one driven by programmable current driver and one 48 VDC power supplied DC motor on the 3th joint. All of them are provided with one incremental encoder and one torque sensor.

Each ESC board is a custom control board featuring an up-to 72 Mhz ARM7 micro-controller, 4 14-bit DAC output interfaces (to set the reference of the current drives), 10 14-bit Analog-to-Digital Converter (ADC) channels (to acquire the torque signals through 2 Wheatstone full-bridge channels that are pre-amplified) and the EtherCAT ET1100 controller linking to double-port Ethernet interface.

III. DYNAMIC MODEL

A. Single joint model

The joints of the exoskeleton can be modeled with a lumped parameter model due to the elasticity of the harmonic drive speed reducer and torque sensor (for joints 1, 2 and 4) and of tendon transmission for joint 3. The used single joint model is a 2-mass with spring and damper (Fig. 5).

The single joint dynamics is formulated by the following equations:

$$\begin{aligned} \underline{\text{J}}\ddot{\theta}_{m,i} + c_{m,i}\dot{\theta}_{m,i} + c_{t,i}(\dot{\theta}_{m,i} - \dot{\theta}_{j,i}) + k_{t,i}(\theta_{m,i} - \theta_{j,i}) &= \tau_{m,i} + \tau_{d,i} \\ \underline{\text{J}}\ddot{\theta}_{l,i} + c_{t,i}(\dot{\theta}_{j,i} - \dot{\theta}_{m,i}) + k_{t,i}(\theta_{j,i} - \theta_{m,i}) &= \tau_{l,i} \end{aligned} \quad (7)$$

where referring to the i -th joint, $\theta_{m,i}$ and $\theta_{j,i}$ stand for motor and joint angles respectively, $k_{t,i}$ and $c_{t,i}$ are the stiffness and viscous coefficient of the transmission, that were experimentally characterized. $\underline{\text{J}}\ddot{\theta}_{m,i}$ is motor inertia, $\underline{\text{J}}\ddot{\theta}_{l,i}$ is average link inertia considered as constant, $\tau_{m,i}$ is the motor torque, $\tau_{d,i}$ is a disturbance torque acting on the motor rotor which accounts for internal friction and ripple effects of both motor and harmonic drive, while $\tau_{l,i}$ is the external torque acting directly on the output link. The $\tau_{l,i}$ torque accounts for the exogenous input due to the interaction with the human, and endogenous input accounting for unmodeled non-linear effects, such as dynamic or gravity forces.

1) *Experimental characterization of single joint performance:* As described in II-A the joint is equipped with a torque sensor that is a part of the transmission chain and is capable of measuring the elastic torque $\tau_{s,i}$, which acts between motor rotor and joint output link. The elastic sensor torque can be expressed by $\tau_{s,i} = k_{t,i}(\theta_{j,i} - \theta_{m,i})$. The joint dynamics can be re-written expliciting the $\tau_{s,i}$ readings starting from $\tau_{s,i}$ definition, its 1st and 2nd derivatives and using the equations 7. It is obtained:

$$\ddot{\tau}_{s,i} + \frac{c_{t,i} c_{t,i}}{J_i I_i} \dot{\tau}_{s,i} + \frac{k_{t,i} k_{t,i}}{J_i I_i} \tau_{s,i} = \frac{k_{t,i} k_{t,i}}{J_l i I_l i} \tau_l + \frac{k_{t,i} k_{t,i}}{J_l i I_l i} \tau_g - \frac{k_{t,i} k_{t,i}}{J_m i I_m i} \tau_m \quad (8)$$

where $J_i = J_l J_m / (J_l + J_m)$, $I_i = I_l I_m / (I_l + I_m)$. The natural frequency of this system is $\omega_n = \sqrt{k_{t,i}/J_i}/2\pi$. The natural frequency has been experimentally evaluated for a single joint in a test-rig analyzing the response of the τ_s when a chirp command is used for the τ_m motor torque.

From Fig. 5, use of the Half-Power Bandwidth method returns $e = 11.8 \text{ Nms/rad}$ $c = 11.8 \text{ Nms/rad}$ as the overall

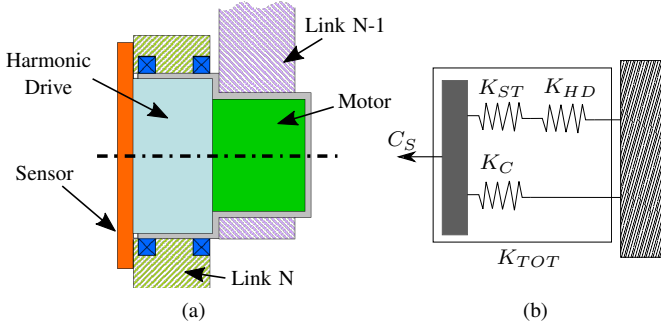


Fig. 4. In a), the schematic representation of the joint. The torque sensor is a series elastic element between the motor and the link n . The torque sensor is not structural and has been designed to transmit only axial torque. In b), the kinematic chain of the joint to non-axial loads. K_{ST} and K_{HD} are the stiffness of the torque sensor and of the Harmonic Drive to non-axial load respectively, whereas K_B is the bearing stiffness.

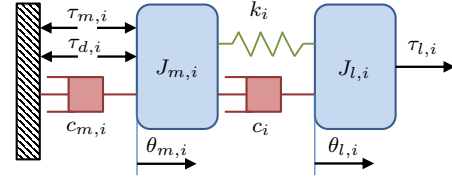


Fig. 5. The 2-mass model for each joint.

TABLE V
THE NATURAL FREQUENCY OF THE JOINTS

Joint	Avg. link inertia [Kg/m ²]	Natural freq. [Hz]
1	0.9639	19.3930
2	1.11	18.3501
4	0.1925	39.6797

damping coefficient of the flexible joint (this value has also been validated via the Logarithmic Decrement method). Con-

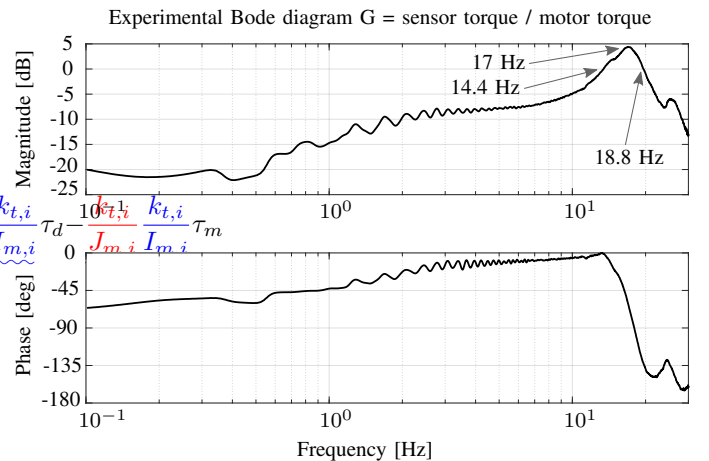


Fig. 6. Experimental open-loop response (Bode magnitude plot) of joints 1, 2 and 4: joint sensor torque vs. motor torque command in standardized testbed conditions.

sidering the exoskeleton, every joint see a link inertia that depends on the pose so the natural frequency of each joint depends on the pose of the exoskeleton. Considering an average link inertia, it can be obtained the natural frequency for each joint elastic transmission. Results are shown in the TABLE V. For all these three joints the motor inertia is the same and it is equivalent to 3.742 Kg/m^2 3.742 Kg/m^2 .

B. Multiple joints model

Given the single joint two-mass model, the dynamic model of the whole exoskeleton can be formulated in matrix form as follows:

$$\left\{ \begin{array}{l} \boxed{\mathbf{I}_m \mathbf{D} \ddot{\boldsymbol{\theta}}_m + \mathbf{B}_m \mathbf{D} \dot{\boldsymbol{\theta}}_m} \xrightarrow{\text{Motor Dynamics}} + \underline{+} \underline{-} + \underline{-} \quad \boxed{\mathbf{C}_t(\mathbf{D} \dot{\boldsymbol{\theta}}_m)} \\ \tau_m + \tau_d \\ () \boxed{\mathbf{M}(\boldsymbol{\theta}) \ddot{\boldsymbol{\theta}} + \mathbf{C}(\dot{\boldsymbol{\theta}}, \boldsymbol{\theta}) \dot{\boldsymbol{\theta}}} \xrightarrow{\text{Joint dynamics}} + \underline{() \quad \mathbf{C}_t(\dot{\boldsymbol{\theta}} - \mathbf{D} \dot{\boldsymbol{\theta}}_m)} \\ + \mathbf{G}(\boldsymbol{\theta}) = \underline{\mathbf{J}^T \mathbf{F}_h} \end{array} \right.$$

where $\mathbf{J_m I_m}$, $\mathbf{B_m}$, \mathbf{D} , $\mathbf{K_t}$ and $\mathbf{C_t}$ are diagonal matrices. $\mathbf{J_m I_m}$ and $\mathbf{B_m}$ model inertia and viscous friction at motor respectively, while $\mathbf{K_t}$ and $\mathbf{C_t}$ model stiffness and damping associated to the elastic transmission and \mathbf{D} models the transmission reduction factor introduced by joint gearheads; $\mathbf{G-G}$ models the effects of gravity force on links. $\mathbf{F_h}$; $\mathbf{F_h}$ are the external forces acting on the system due to human interaction and the respective joint torques are computed by multiplying them by the transposed Jacobian matrix $\mathbf{J^T J^T}$ evaluated in the actual exoskeleton configuration. The multi-joint model introduces cross-coupling among joints and nonlinearities, with terms $\mathbf{C}(\dot{\theta}_j, \theta_j) \mathbf{C}(\dot{\theta}, \theta)$ that models Coriolis effects and $\mathbf{M}(\theta_j) \mathbf{M}(\theta)$ that represents links inertia.

By taking into account that the real dynamics has terms $M(\theta_j)$ and $C(\dot{\theta}_j, \theta_j)$ depending on the actual joint configuration, the first term can be decoupled and that can be decomposed into a diagonal constant component and a variable component as follows:

$$\mathbf{M}\ddot{\boldsymbol{\theta}} = \overline{\mathbf{M}}\ddot{\boldsymbol{\theta}}_{\text{constant}} + \underline{\Delta(\boldsymbol{\theta})} \Delta\mathbf{M}(\boldsymbol{\theta})\ddot{\boldsymbol{\theta}}_{\text{variable}} \quad (10)$$

and introducing the following variable substitution for joint torque τ_s . By making a replacement of variables introducing this expression for the joint torque

$$\left\{ \begin{array}{l} \tau_s = -K_t(D\theta_m - \theta) \\ \end{array} \right. = \underline{\underline{(-)}} = \underline{\underline{(-)}} \quad (11)$$

the dynamics equations (9) can be reformulated as follows
in terms of new variables τ_s and θ_m :

$$\left\{ \begin{array}{l} \cdot =^{-1} + + + + -^{-1} + -^{-1} =^{-1} + + -^{-1} T -^{-1} - -^{-1} . \end{array} \right.$$

where \mathbf{u} (see appendix) represents the actual control command and the external disturbance forces have been collected within the external load force \mathbf{F}_l term (see Appendix I for detailed derivation of terms).

This form of the dynamics equation is useful for defining a full-state feedback control law and an optimal observer for the estimation of joint torque.

1) Joint acceleration estimation: The full dynamics model of the exoskeleton is dependent on the acceleration of each joint. In order to estimate and compensate for the dynamics of the device, an observer for the joint acceleration has been designed. The observer estimates the acceleration from motor

encoder $\theta_{m,i}$, joint torque $\tau_{s,i}$ and the imposed control torque $\tau_{m,i}$. $\tau_{s,i}$ is the torque measured by the sensor at the joint and can be expressed as in equation (12):

The acceleration can be estimated starting from a model of the actuation group (motor and gearbox), in particular by modeling the torque acting on the actuation group as $K_t(\theta - D_m)$ (Elastic transmission torque + $(+) + (-) +$) and by considering the losses as a static and a velocity-dependent viscous friction. Thus, the acceleration can be estimated as:

$$\begin{cases} \ddot{\theta}_{m,i} = 0 & \text{for } -\tau_{A,i} < \tau_{m,i} - \tau_{s,i} < \tau_{A,i} \\ \ddot{\theta}_{m,i} = \frac{\tau_{m,i} - \tau_{s,i} - c_{m,i}\dot{\theta}_{m,i}}{J_{m,i}} & \text{otherwise} \end{cases} \quad (13)$$

where $\tau_{A,i}$ is the static friction torque and $c_{m,i}$ is the dynamic friction coefficient that were experimentally evaluated. The torque saturation effects due to power supply voltage limits are modeled as:

$$k_c \frac{-V_{max} - k_v \dot{\theta}_{m,i}}{R} < \tau_{m,i} < k_c \frac{V_{max} - k_v \dot{\theta}_{m,i}}{R} \quad (14)$$

depending on the electric constants of each motor, and in particular where k_c is the associated torque constant, k_v is the velocity constant, R is the winding terminal resistance and V_{max} is the maximum supply voltage to the motor. An optimum **Kalman**-observer has been used to estimate the acceleration term $\ddot{\theta}_{m,i}$ and a diagram of the estimation of acceleration by using control and measured torques is shown in Fig. 7.

The model can be expressed in the state variable form as follows:

$$\begin{cases} \dot{\mathbf{x}} = \mathbf{A}\mathbf{x} + \Gamma\mathbf{d} \\ \mathbf{y} = \mathbf{C}\mathbf{x} \end{cases} \quad (15)$$

where

$$x = \begin{bmatrix} \theta_{m,i} \\ \dot{\theta}_{m,i} \\ \ddot{\theta}_{m,i} \end{bmatrix} \mathbf{A} = \begin{pmatrix} 0 & 1 & 0 \\ 0 & 0 & 1 \\ 0 & 0 & 0 \end{pmatrix} \Gamma = \begin{bmatrix} 0 \\ 0 \\ 1 \end{bmatrix} \mathbf{C} = \begin{pmatrix} 1 & 0 & 0 \\ 0 & 0 & 1 \end{pmatrix} \quad (16)$$

and \tilde{d} is the process noise.

$$\begin{aligned} \text{The observer can be formulated as:} \\ \mathbf{s} + \mathbf{K}_t \mathbf{i}_t^{-1} \boldsymbol{\tau}_s = \mathbf{K}_t \mathbf{i}_m^{-1} (\mathbf{L}_m \bar{\mathbf{M}}^{-1} \mathbf{J}^T \mathbf{E}_t \dot{\mathbf{x}}) \quad (12) \\ \boldsymbol{\tau}_s = \mathbf{u} \quad (17) \end{aligned}$$

where L is the gain matrix of the observer. A scheme of the observer is depicted in figure (??). Block diagram of the acceleration observer

The gain L was found resolving the problem of a Kalman optimum observer based on the experimental covariance data of measurement and process noise. Measurement noise was derived from motor encoder $\theta_{m,i}$ measurements, that mainly takes into account the encoder quantization and motor acceleration $\dot{\theta}_{m,i}$ estimation through (13), thanks to the available torque measurement.

As an example, the comparison between the real-time estimated acceleration (red dotted line) and the off-line calculated acceleration (blue solid line) for the first two joints is shown in figure 8.

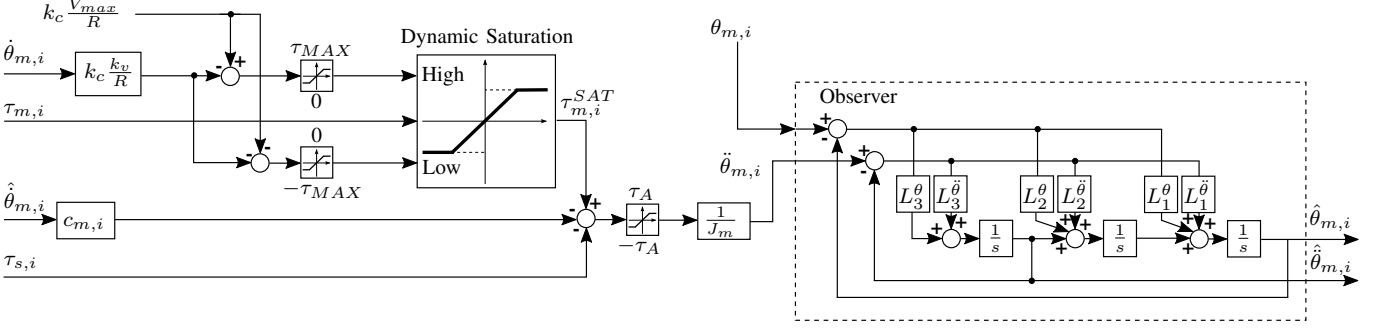


Fig. 7. Estimation of the acceleration from torque measurement.

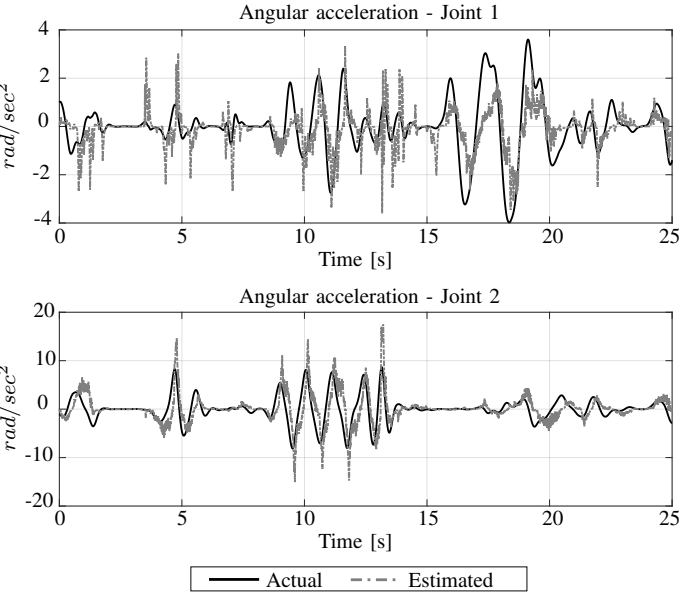


Fig. 8. Comparison between the estimated and actual acceleration

2) *Dynamics compensation:* As reported by equation (21), the torques measured by joint sensors are due to the human force and any load applied on the links (\mathbf{F}_l). To have a good estimation of human forces by torque sensors, it is necessary to remove from torque measurements the gravity and dynamics loads applied to the links. The gravity contribution depends only on the pose of the exoskeleton and it can be calculated by the position signals provided by the motor encoders. The gravitational term is already compensated in feed-forward by the term $\hat{\mathbf{G}}(\mathbf{D}\hat{\theta}_m)\hat{\mathbf{G}}(\mathbf{D}\hat{\theta}_m)$ in τ_m , except for the term $\delta g\delta g$. On the other side, the dynamics contribution depends both on the pose and the acceleration and velocity of the links, which are not directly provided by any sensor, but are provided in first approximation as $\mathbf{D}\hat{\theta}_m\mathbf{D}\hat{\theta}_m$ by the observer described in section III-B1.

The dynamics torques due to the links inertia and measured by the joint torque sensors can be so estimated as the sum of the inertial contribute and the Coriolis effect:

$$\hat{\tau}_{dyn}\hat{\tau}_{dyn} \approx \hat{\mathbf{M}}(\mathbf{D}\theta_m)\mathbf{D}\ddot{\theta}_m + \hat{\mathbf{C}}(\mathbf{D}\theta_m, \mathbf{D}\dot{\theta}_m)\mathbf{D}\dot{\theta}_m \quad (18)$$

where matrices $\hat{\mathbf{M}}$ and $\hat{\mathbf{C}}$ are calculated taking into account for each joint the inertia of the parts supported by the torque sensor, discarding the inertia of the actuator of the joint.

The estimated dynamic torques are then used to compensate the dynamic effects of the link: the compensation torques $\alpha\hat{\tau}_{dyn}\hat{\tau}_{dyn}$, with $0 < \alpha < 1$, are a percentage of the estimated torques $\hat{\tau}_{dyn}\hat{\tau}_{dyn}$. The compensation torques are added to the desired torques $\tau_s^D\tau_s^D$ as input to the state feedback controller and feed-back with the estimated torque $\hat{\tau}_s\hat{\tau}_s$.

III. DISCUSSION

The results highlight the advantages of using a full-state feedback controller that compensates also for estimated disturbance torques and for viscous torque losses of the motor. The major benefit on the use of the full state feedback control is high exhibited transparency during the free motion task. This means that the exoskeleton can affect less the user desired motion and at the same time the robot is able to more accurately identify the user intention (the human forces/torques).

Although the basic state feedback control (JTFC2) presents an average force modulus at the end-effector similar to the passivity-based feedback control (JTFC3), it hinders the user voluntary motion more than the other controls do. In fact the end-effector trajectory due to the control JTFC2 is the farthest from the desired one. This is because the JTFC1 and the JTFC3 take into account (although different ways) both the link's inertia and the motor's inertia, whereas the JTFC2 control considers only the motor's inertia. The full state controller explicitly estimates the load torques and feed-forwards this contribution by multiplying it by a gain. On the other side, the passivity-based controller imposes by control the desired link's inertia, thus this is a direct objective of the control.

The high transparency (the average force modulus at the end-effector is less than 6 N for JTFC1) is also due to the effect of the dynamic compensations. A correct estimation of the joint acceleration is crucial to obtain a transparency enhancement, this is the reason why the dynamic contributions are weighted by a constant less than 1. In fact only with a perfect acceleration estimation *it a high transparency can*

be obtained a high transparency keeping a exhibiting a stable behavior. The proposed methodology for the estimation of the acceleration through torque sensor's data and motor's data can help to improve the acceleration calculation estimation.

An important result is the wide range of stable impedances that the system can render is capable of rendering. The Rehab-Exos was able to render a flat surface with a stiffness equal to 40 kN/m with all the three compared control laws with different performances performance but still preserving stability. This is certainly due to inherent mechanical damping of the system.

The mechanical design of the exoskeleton influences its performances performance. The residual torques at the joint are basically the effects of the unmodeled link inertia and the joint friction. A more light design made by small motors and small lighter design obtained with smaller motors and lower transmission ratio will lead to a more backdrivable solution with at the price of a less torque available at the joint. This could be a solution to experience an even trade-off solution to achieve a more transparent device. Moreover Last but not least the torque sensor requires a more robust design; more in detail, to obtain a smaller sensitivity to non-axial loads a spoke with wider beams can be implemented.

The choice of a joint with an active impedance by control based on a torque sensor presents a valid alternative to the passive inherent compliant actuators in order to achieve a more compact and simpler mechanics and electronics. The proposed torque control combined with the joint mechanics allow to build allows building safe and responsive control strategies suitable for rehabilitation and assistance.

IV. CONCLUSION

This paper presents the Rehab-Exos exoskeleton design and in particular the design of the joint torque sensors based on strain gauges. Some sensor's issue have been explained and two possible hypotheses have been proposed. Then an interaction torque control has been developed and validated by experimental tests such as the transparency test and the haptic interaction tasks. The kinematics and dynamics of the device are calculated by a full dynamics model implemented in a centralized torque control. The torque tracking for each joint is performed by single-joint full-state Kalman filter and a torque feedback controller. The centralized control provides to each single-joint observer the desired torque for force feedback and an estimation of the joint torques due to links dynamic loads to be compensated by the control as feed-forward contributions. The developed full-state feedback control was then compared with a basic feedback control and a passivity-based feedback control. Results show how the full-state approach is effective for estimating the human interaction force cleaned up of the inertial and gravity contributions due to the non negligible mechanical properties of the exoskeleton structure. The full-state feedback control is more accurate and transparent than the other two controls. The proposed control strategy combined with the presence of a joint torque sensor can enhance the performances of the human-robot interaction based on exoskeleton even in presence of non backdrivability.

ACKNOWLEDGMENTS

The authors would like to thank Marco Graffiedi for his contribute on the study of the torque sensor cross-talk reading.

V. APPENDIX I

Let us study the effect under static condition of the application of a motor torque compensating for the non-linearity due to gravity, estimated as $\hat{\mathbf{G}}(\mathbf{D}\hat{\theta}_m)\hat{\mathbf{G}}(\mathbf{D}\hat{\theta}_m)$, with:

$$\underline{\tau_m} \underline{\tau_m} = \hat{\mathbf{G}}(\mathbf{D}\hat{\theta}_m) + \mathbf{u} \quad (19)$$

where $\underline{\mathbf{u}}$ represents the actual control command. Under static conditions it can be found that:

$$\underline{\mathbf{u}}\underline{\mathbf{u}} = -\mathbf{J}^T \mathbf{F}_h + \mathbf{G}(\boldsymbol{\theta}) - \hat{\mathbf{G}}(\mathbf{D}\hat{\theta}_m) \approx -\mathbf{J}^T \mathbf{F}_h \quad (20)$$

since $\hat{\mathbf{G}}(\mathbf{D}\hat{\theta}_m) \approx \mathbf{G}(\boldsymbol{\theta}_j)\hat{\mathbf{G}}(\mathbf{D}\hat{\theta}_m) \approx \mathbf{G}(\boldsymbol{\theta})$. Under dynamic conditions, the incomplete cancellation of the gravity component due to the elasticity of the joint transmission can be modeled by introducing a disturbance term $\delta g = \mathbf{G}(\boldsymbol{\theta}_j) - \hat{\mathbf{G}}(\mathbf{D}\hat{\theta}_m)\delta g = \mathbf{G}(\boldsymbol{\theta}) - \hat{\mathbf{G}}(\mathbf{D}\hat{\theta}_m)$, that can be summed up to \mathbf{F}_h as a disturbance noise supported by the operator.

So a variable apparent dynamic force $\underline{\mathbf{F}_{dyn}}$ can be defined such that $\mathbf{J}^T \Delta \mathbf{F}_{dyn}(\dot{\boldsymbol{\theta}}_j, \boldsymbol{\theta}_j) = -\Delta \mathbf{M}(\boldsymbol{\theta}_j)\ddot{\boldsymbol{\theta}}_j - \mathbf{C}(\dot{\boldsymbol{\theta}}_j, \boldsymbol{\theta}_j)\dot{\boldsymbol{\theta}}_j$ $\mathbf{J}^T \Delta \mathbf{F}_{dyn}(\boldsymbol{\theta}, \boldsymbol{\theta}) = -\Delta \mathbf{M}(\boldsymbol{\theta})\ddot{\boldsymbol{\theta}} - \mathbf{C}(\dot{\boldsymbol{\theta}}, \boldsymbol{\theta})\dot{\boldsymbol{\theta}}$. The new variable $\Delta \mathbf{F}_{dyn}$, representing uncompensated and/or unmodeled dynamics, can be considered as a disturbance force and considered as a contribution term to the overall external load force $\underline{\mathbf{F}_l}$ expressed by:

$$\underline{\mathbf{F}_l} \underline{\mathbf{F}_l} = \underline{\mathbf{F}_h} \text{ exogenous} + \underline{\delta g} + \underline{\Delta \mathbf{F}_{dyn}} \text{ endogenous} \quad (21)$$

This in general states that the external forces are the sum of exogenous \mathbf{F}_h and endogenous inputs $\delta g + \Delta \mathbf{F}_{dyn}$. While exogenous inputs are unknown a priori and depending on human operator behavior, endogenous inputs can be estimated and compensated to some extent.

So introducing the variable substitution expressed by (12), dynamic equations can be reformulated as follow:

$$\mathbf{I}_m \mathbf{D}\ddot{\boldsymbol{\theta}}_m + \mathbf{B}_m \mathbf{D}\dot{\boldsymbol{\theta}}_m \pm = \mathbf{C}_t \mathbf{K}_t^{-1} \dot{\boldsymbol{\tau}}_s + \boldsymbol{\tau}_s + \mathbf{u} + \boldsymbol{\tau}_d \quad (22)$$

$$\bar{\mathbf{M}}\ddot{\boldsymbol{\theta}} + \mathbf{C}_t \mathbf{K}_t^{-1} \dot{\boldsymbol{\tau}}_s + \boldsymbol{\tau}_s = \mathbf{J}^T \mathbf{F}_l \quad (23)$$

But we know that

$$\mathbf{K}_t^{-1} \dot{\boldsymbol{\tau}}_s + \mathbf{D}\ddot{\boldsymbol{\theta}}_m = \ddot{\boldsymbol{\theta}} \quad (24)$$

Then making substitution of (24) in (23) to eliminate $\boldsymbol{\theta}_j$ and its higher order derivatives $\dot{\boldsymbol{\theta}}$, we obtain:

$$\underline{\mathbf{MD}} \underline{\mathbf{D}\ddot{\boldsymbol{\theta}}_m} + \bar{\mathbf{MK}}_t^{-1} \dot{\boldsymbol{\tau}}_s + \mathbf{C}_t \mathbf{K}_t^{-1} \dot{\boldsymbol{\tau}}_s + \boldsymbol{\tau}_s = \mathbf{J}^T \mathbf{F}_l \quad (25)$$

and then replacing $\mathbf{D}\ddot{\theta}_m = \mathbf{J}_m^{-1} \{-\mathbf{B}_m \mathbf{D}\dot{\theta}_m + \mathbf{K}_t^{-1} \mathbf{C}_t \dot{\tau}_s +$
and defining $\mathbf{J}_i^{-1} = \bar{\mathbf{M}}^{-1} [\mathbf{I} + \bar{\mathbf{M}} \mathbf{J}_m^{-1}]$ from (22)
 $\mathbf{D}\ddot{\theta}_m = \mathbf{I}_m^{-1} \{-\mathbf{B}_m \mathbf{D}\dot{\theta}_m + \mathbf{C}_t \mathbf{K}_t^{-1} \dot{\tau}_s + \tau_s + u + \tau_d\}$
and defining $\mathbf{I}_i^{-1} = \bar{\mathbf{M}}^{-1} + \mathbf{I}_m^{-1}$, dynamics equations can
be put in the following form:

$$\begin{aligned} \mathbf{J}_m \mathbf{D}\ddot{\theta}_m + \mathbf{B}_m \mathbf{D}\dot{\theta}_m &= \mathbf{K}_t^{-1} \mathbf{C}_t \dot{\tau}_s + \tau_s + u + \tau_d \\ \ddot{\tau}_s + \mathbf{C}_t \mathbf{I}_i^{-1} \dot{\tau}_s + \mathbf{K}_t \mathbf{I}_i^{-1} \tau_s &= \mathbf{K}_t \bar{\mathbf{M}}^{-1} \mathbf{J}_i^T \mathbf{F}_1 \\ &+ \mathbf{K}_t \mathbf{I}_m^{-1} (\mathbf{B}_m \mathbf{D}\dot{\theta}_m - \tau_d - u) \end{aligned} \quad (26)$$

This form of the dynamics equation is useful for defining a full-state feedback control law and an optimal observer for the estimation of joint torque.

REFERENCES

- [1] M. Hashimoto and Y. Kiyosawa, "Experimental study on torque control using harmonic drive built-in torque sensors," *Journal of Robotic Systems*, vol. 15, no. 8, pp. 435–445, 1998.
- [2] A. Kugi, C. Ott, A. Albu-Schaffer, and G. Hirzinger, "On the passivity-based impedance control of flexible joint robots," *Robotics, IEEE Transactions on*, vol. 24, no. 2, pp. 416–429, 2008.
- [3] R. Vertechy, A. Frisoli, M. Solazzi, D. Pellegrinetti, and M. Bergamasco, "An interaction-torque controller for robotic exoskeletons with flexible joints: Preliminary experimental results," in *Intelligent Robots and Systems (IROS), 2012 IEEE/RSJ International Conference on*. IEEE, 2012, pp. 335–340.



Domenico Chiaradia received the B.S. and M.S. degrees with honours in control theory and automation engineering from the Polytechnic University of Bari, Italy, in 2011 and 2014 respectively. He is currently pursuing the Ph.D. degree in robotics engineering at Perceptual Robotics (PERCRO) Laboratory, TeCIP Institute, Sant'Anna School of Advanced Studies, Pisa, Italy. His research interest includes control of rigid and soft exoskeletons for assistance and rehabilitation, torque control, control of haptic interfaces and physical human-robot interaction.



Massimiliano Solazzi (Eng., Ph.D.) is Assistant Professor in Applied Mechanics at the Sant'Anna School of Advanced Studies in Pisa, Italy. He carries out his research at the Percro laboratory - TeCIP. In 2010 he received the PhD Degree in Innovative Technologies from the Sant'Anna School of Advanced Studies. His research interests concerns: the design of robotic interfaces for virtual reality, teleoperation and rehabilitations, and the psychophysical validation of HMI.



Rocco Vertechy (Eng., Ph.D.) is Associate Professor at the Industrial Engineering Department of the School of Engineering and Architecture of the University of Bologna in Italy, where he leads the group on advanced actuation technologies and renewable energy robotic systems. He is Mechanical Engineer (2001) and PhD in Mechanics of Machines (2005). He was: Research Assistant at the Department of Mechanical Engineering, University of Canterbury (New Zealand); Visiting Researcher at the Robotics Locomotion Laboratory, Stanford University (California); Contract Professor at the University of Bologna; Assistant Professor at the Perceptual Robotics Laboratory of the Scuola Superiore Sant'Anna (Italy).



Antonio Frisoli (Eng., PhD) is Professor of Robotics and Mechanical Engineering at the Sant'Anna School of Advanced Studies, Pisa-Italy, where he is head of the Human-Robot Interaction area at PERCRO laboratory of TeCIP Institute. He received his PhD (2002) with honors in Industrial and Information Engineering from the Sant'Anna School of Advanced Studies, Italy and the MSc (1998) in Mechanical Engineering, minor Robotics, from University of Pisa-Italy. He has been chair of the IEEE Technical Committee on Haptics, the general chair of the Eurohaptics 2018 conference in Pisa and Human-Machine Interaction summer school HMISS 2017. In the field of robotics and haptics he acts as associated editor in numerous international conferences, such as IEEE Worldhaptics, IEEE Roman, IEEE Haptic Symposium among many others, and journals, such as IEEE Robotics and Automation Letters and MIT Press Presence.